Improving Charge Separation Across a Hybrid Oxide/Polymer Interface by Cs Doping of the Metal Oxide

Yunus Sevinchan,[a][b] Paul E. Hopkinson,[a][b] Artem A. Bakulin,[c] Julia Herz,[d] Marcus Motzkus[d][b] and Yana Vaynzof [a][b]*

[a] Kirchhoff-Institute for Physics, Im Neuenheimer Feld 227, Heidelberg University, Germany

[b] Centre for Advanced Materials, Im Neuenheimer Feld 225, Heidelberg University, Germany

[c] Cavendish Laboratory, JJ Thomson Ave, University of Cambridge, UK

[d] Institute of Physical Chemistry, Im Neuenheimer Feld 229, Heidelberg University, Germany

*email: vaynzof@uni-heidelberg.de

Abstract: The process of photoinduced charge carrier separation in hybrid optoelectronics remains only partially understood, with the mechanism behind creation and dissociation of bound charge pairs (BCPs) being open questions. To investigate these processes, we employ the model hybrid ZnO/P3HT system and show that Cs doping of ZnO results in a decrease in the density of gap states at the metal oxide surface and in turn, a reduction in the yield of BCPs. This provides direct experimental evidence for a previously proposed model of BCP creation by electron trapping at the metal oxide surface states. Furthermore, Cs doping is found to substantially increase open circuit voltage in these devices without the negative effects on short circuit current that were observed in studies with other dopants. This offers new possibilities for hybrid photovoltaic devices with increased power conversion efficiencies and provides valuable insights on the charge separation processes in hybrid organic-inorganic photovoltaics.

Introduction

Hybrid organic-inorganic photovoltaic devices typically consist of an organic conjugated polymer that serves as the light absorber and donor, and an inorganic acceptor – usually a metal oxide. These devices offer the possibility to combine the advantages of both organic and inorganic materials and explore the possibility of replacing fullerene derivatives in organic photovoltaics.[1–3] However, despite a decade of research, the efficiencies of hybrid photovoltaic devices remain low and the charge separation process at the hybrid interface is not entirely understood.

It was previously observed that photoinduced charge transfer at the organic-inorganic interface of hybrid photovoltaic devices does not solely result in free charge carriers but also in bound electron-hole pairs. These bound charge pairs (BCPs) later recombine and do not contribute to the photocurrent, thus lowering device performance. It was proposed that defect states at the surface of the metal oxide might be the cause of BCPs, with the localized electron coulombically attracting and holding the hole polaron close to the interface.[4] However, no experimental evidence for the connection between surface defect states and BCPs was presented to date.

Several approaches to improve the photovoltaic device performance were investigated in literature, including modification of the interface with a self-assembled monolayer (SAM), metal oxide doping or a combination of both. In ZnO, for example, a variety of dopants have been investigated including Mg,[5,6] N,[7] Sr,[8] and Ca[9]. When examining the performance of a bilayer doped ZnO/P3HT device, the increase in performance comes as a result of increased open circuit voltage, either by raising the conduction band level of the metal oxide or by reducing its conductivity and thus, the device dark current. An increase in short circuit current is reported to result from increased surface roughness of the metal oxide, which increased the interfacial area where charge separation can take place.[5,9] Alternatively, modification of the ZnO surface with a dye or a SAM typically results in an increase in short circuit current of the device.[4,10–14] It was recently demonstrated that a combination of Sr doping

and SAM modification can significantly improve charge separation and performance of the hybrid photovoltaic device.[8]

The present study shows that Cs doping of ZnO allows for controlled reduction of the number of gap states at the surface of the metal oxide as probed by ultraviolet photoemission spectroscopy. Pump-push photocurrent spectroscopy was employed to demonstrate that this decrease of gap states suppresses the formation of BCP states at the hybrid metal oxide/polymer interface. The reduction in BCP states was confirmed by monitoring the increase in population of free charges by transient absorption spectroscopy. These results elucidate the mechanism for BCP formation by localization of electrons at metal oxide surface states, and demonstrate that efficient charge separation can be achieved in a hybrid photovoltaic system by reducing the number of gap states. Additionally, Cs doping results in a significant increase in the open circuit voltage due to a reduced conductivity of the ZnO, which leads to a decrease in the device dark current. The combination of these beneficial changes in the bulk and surface properties of ZnO resulted in a power conversion efficiency of 0.63 % for a bilayer device, exceeding the reported 0.4 % for P3HT/PCBM bilayer devices.[15]

Results and Discussion

Effects of Cs doping on P3HT/ZnO:Cs hybrid photovoltaic device performance

Bilayer hybrid photovoltaic devices were prepared in the inverted architecture and with varying levels of Cs doping in the ZnO layer. Figure 1 shows the device architecture and the chemical structures of precursors used in solution processing of these devices. The incorporation of Cs into the ZnO layer (in the following called *doping*) by adding Cs_2CO_3 to the sol-gel was confirmed by X-ray photoemission spectroscopy. The doping level in the film could be controlled by the amount of Cs_2CO_3 added in solution (Figure S1, SI). The doping levels are given in % molar ratio (%MR) of Cs to Zn atoms, i.e. # Cs atoms / # Zn atoms in the precursor solution.
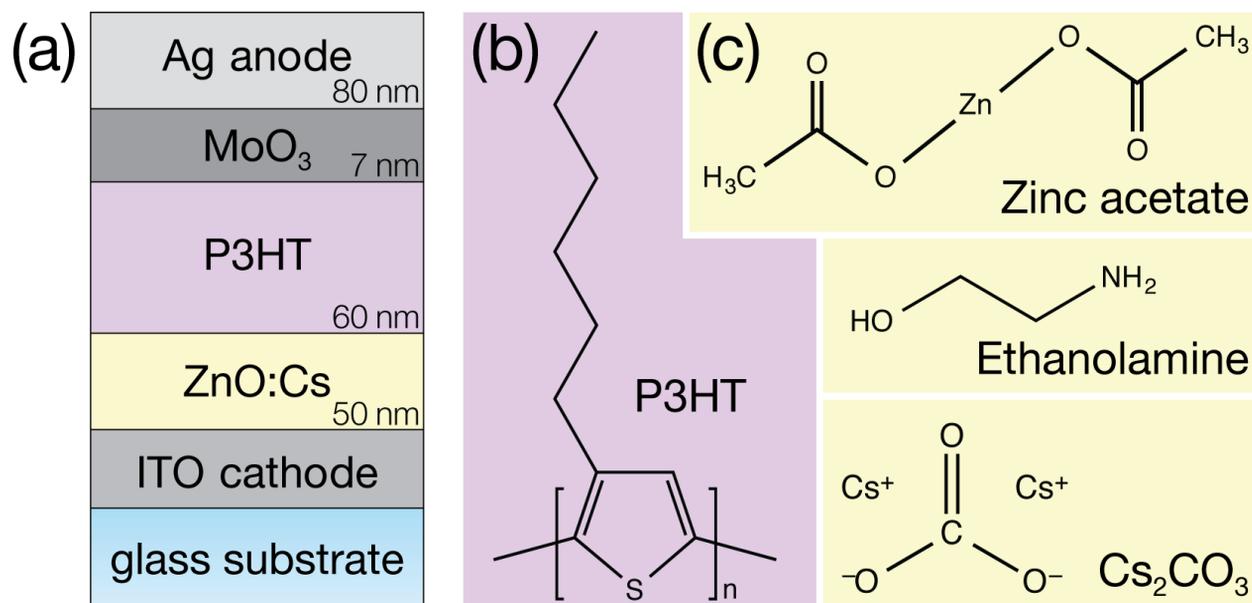
Figure 1: **(a)** Cross section of the inverted bilayer architecture. Light is incident through the glass substrate and the transparent ITO cathode and ZnO:Cs electron acceptor layer. **(b)** Chemical structure of Poly-[3-hexylthiophene] (P3HT), **(c)** precursors for the ZnO layer (zinc acetate and monoethanolamine) and Cs_2CO_3 used for doping.
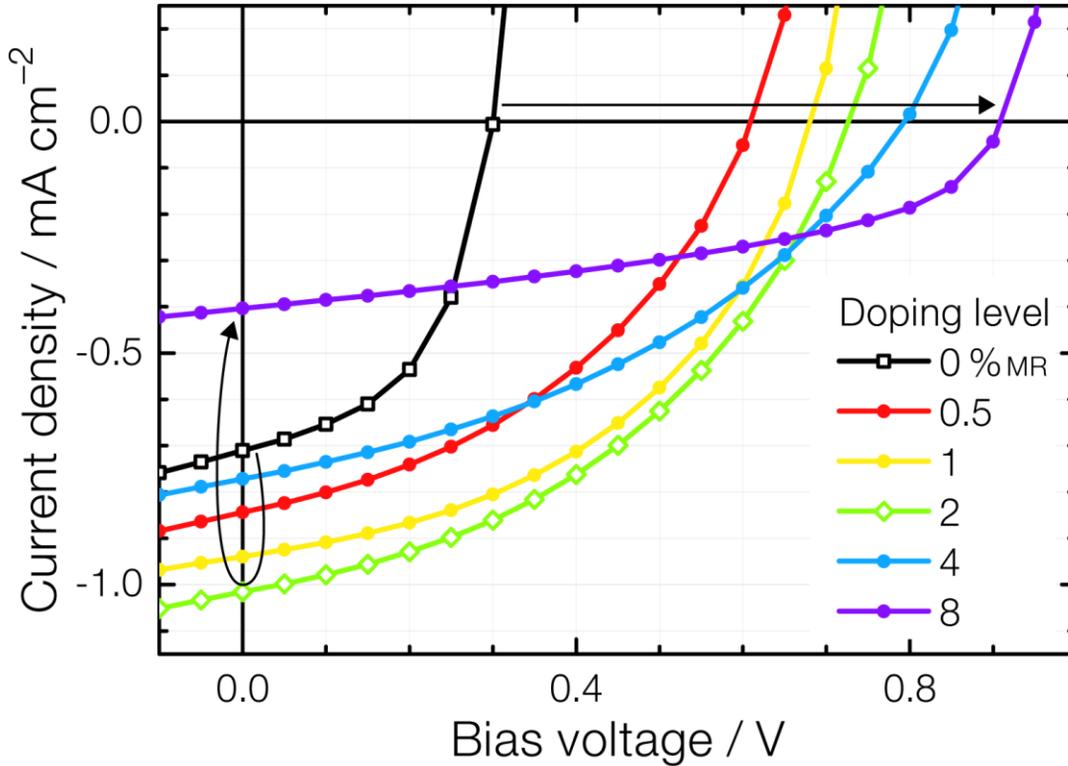
Figure 2: *J-V* characteristics of representative hybrid ZnO:Cs/P3HT photovoltaic devices with increasing Cs doping level, measured under mismatch-corrected AM 1.5G conditions with $100\,mW\,cm^{-2}$ light intensity. Comparing the undoped device (open squares) with the optimally doped device (open diamonds) shows the increase in power conversion efficiency upon doping.

Representative *J-V* curves for Cs doping levels ranging from 0 %MR to 8 %MR are presented in Figure 2. Devices from the same production batch only showed small variations in the photovoltaic metrics (see Figure S2, SI). As similarly observed for other dopants such as Mg,[2] Sr,[8] and Ca,[9] the open circuit voltage (V_{OC}) of the devices significantly increases from 0.3 V, for undoped ZnO devices, up to 0.9 V for 8 %MR Cs doping. In addition to the increase in V_{OC}, an increase in short circuit current (J_{SC}) for low doping levels of up to 2 %MR was observed. With further increase in the doping level the J_{SC} decreases significantly. EQE measurements showed that the increase and decrease in photocurrent

occured uniformly over the spectrum (see Figure S3, SI). The optimal doping level with respect to the highest power conversion efficiency (PCE) was consistently observed between 1 %MR and 2 %MR, coinciding with the highest values for the J_{SC}.

As the V_{OC} depends on the energetic difference between the HOMO level of the polymer and the conduction band of the ZnO, an increase in conduction band edge position would increase the V_{OC} of the device; so if the conduction band of ZnO shifts upon Cs doping, this would explain the V_{OC} increase observed above. This mechanism was demonstrated by Olson et al. using Mg doping of ZnO: through a doping induced offset of the metal oxide conduction band the V_{OC} was increased by 0.4 V.[5] Wang et al. showed that a somewhat smaller increase of 0.24 V in V_{OC} can be achieved by Ca doping due to a similar shift in the oxide conduction band.[9] A comparable increase in V_{OC} was achieved by Hoye et al. for Mg doped ZnO/PbSe quantum dot solar cells.[16]
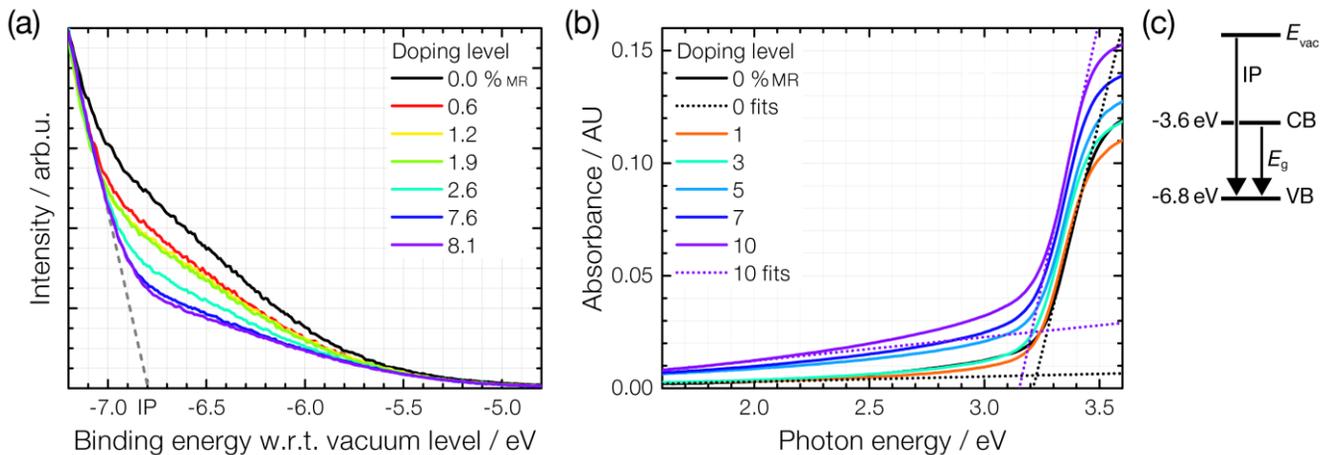
Figure 3: (a) Ultraviolet photoemission spectroscopy (UPS) measurements and determination of the ionization potential (IP) of undoped and Cs doped ZnO. **(b)** UV-vis measurements of undoped and Cs doped ZnO films, from which the optical band gap (E_g) was computed via a fit to the absorption onset and the background (only shown for for 0 %MR and for 10 %MR). **(c)** Energy level diagram summarizing the values extracted from UPS and UV-vis measurements.

To investigate the effect of Cs doping on the energy levels of ZnO, ultraviolet photoemission spectroscopy (UPS) measurements were performed to extract the position of the valence band. Figure 3a shows the UPS spectra of undoped and Cs doped ZnO films for a variety of doping levels. We interpret the low binding energy edge of the UPS spectrum as corresponding to the valence band position.[17] Within the uncertainty of the measurement, no change in the ionization potential (IP, marked by the dotted line) was observed, and a mean value of (6.8 ± 0.1) eV for the ionization potential was determined. These IP values were consistent across a range of samples and sample positions as well as previous measurements; the error is that intrinsic to UPS measurements.[8,10,18,19] The position of the conduction band edge can be found by substracting the optical gap, as it represents a good approximation for the transport gap due to the low exciton binding energy of ZnO (~ 60 meV) compared to its transport gap.[20–22] Figure 3b shows the UV-vis absorption spectra of ZnO films for various Cs doping levels. The optical band gap was determined by a linear fit to the absorption onset and the background and was found to be independent of the doping level, yielding a mean value of (3.20 ± 0.05) eV.

It can be concluded that the energy level alignment of doped ZnO (summarized in Figure 3c) is unaffected by the introduction of Cs, as neither the ionization potential nor the optical band gap was found to change significantly with increasing doping level (see Figure S4, SI). Thus, the increase in V_{OC} is not caused by a change in energy level alignment.
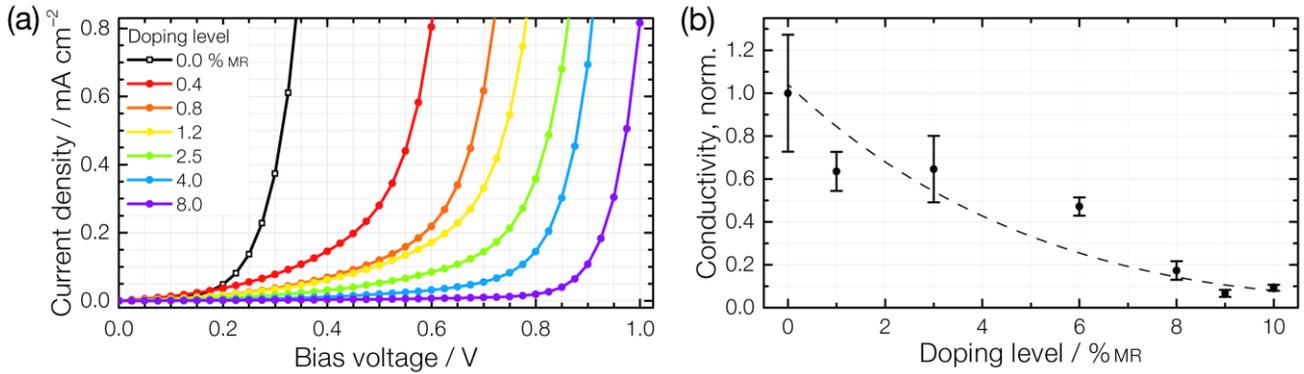
Figure 4: (a) *J-V* characteristics of ITO/ZnO:Cs/P3HT/MoO$_3$/Ag diodes with various doping levels measured in the dark. **(b)** Conductivity of ZnO:Cs films determined by a planar two point probe measurement for different Cs doping levels, normalized to the conductivity of the undoped ZnO layer (line to guide the eye)

As the energy levels of the ZnO do not shift with doping, there must be another cause for the shift in V_{OC} with Cs doping. In Sr doped ZnO, a change in conductivity was determined to cause an increase in V_{OC}, by reduction of the device dark current. The ITO/ZnO:Cs/P3HT/MoO$_3$/Ag devices do show a lower dark current with increasing doping level (Figure 4a), so two point probe conductivity measurements were performed and confirmed a decrease in conductivity with doping (Figure 4b). The decrease in conductivity upon doping (Figure 4b) suggests a lower concentration of intrinsic charge carriers in Cs doped ZnO films.[23]

While an increase in the open circuit voltage upon doping or interface modification of the ZnO layer was previously observed[8] and thus also expected for Cs doping, an increase in the short circuit current density (J_{SC}) of the investigated hybrid photovoltaic devices was not: in studies with Sr doping,[8] and Mg doping,[24] the J_{SC} was found to decrease with increasing doping. On the other hand, an increase in J_{SC} was found in the case of Ca doping[9] and Mg doping[5] to result from increased surface area of the hybrid interface due to a large surface roughness of the doped films. In both cases, the authors report

that the increase in J_{SC} is followed by a decrease at high doping levels due to higher series resistance of the metal oxide.

In the case of Cs doping the decrease in J_{SC} can also be explained by the decrease in conductivity of the metal oxide (Figure 4a). However, the initial increase in J_{SC} cannot be attributed to an increase in surface area, as confirmed by atomic force microscopy: although the roughness and surface area were found to slightly increase with doping level, the change in surface area is too small to explain the observed increase in device current (3 % higher surface area, ~40 % higher current at 2 %MR doping level; see Figure S5, SI). For comparison, the roughness for Ca doped ZnO films was reported to be as high as 45 nm, rising from 4 nm for undoped ZnO.[9] Therefore, an increase in the surface area of Cs doped ZnO films can be excluded as the reason for the improvement in the short circuit current; the increase is proposed to be a result of a more efficient exciton dissociation that is facilitated by decreased BCP formation at the ZnO:Cs/polymer interface.
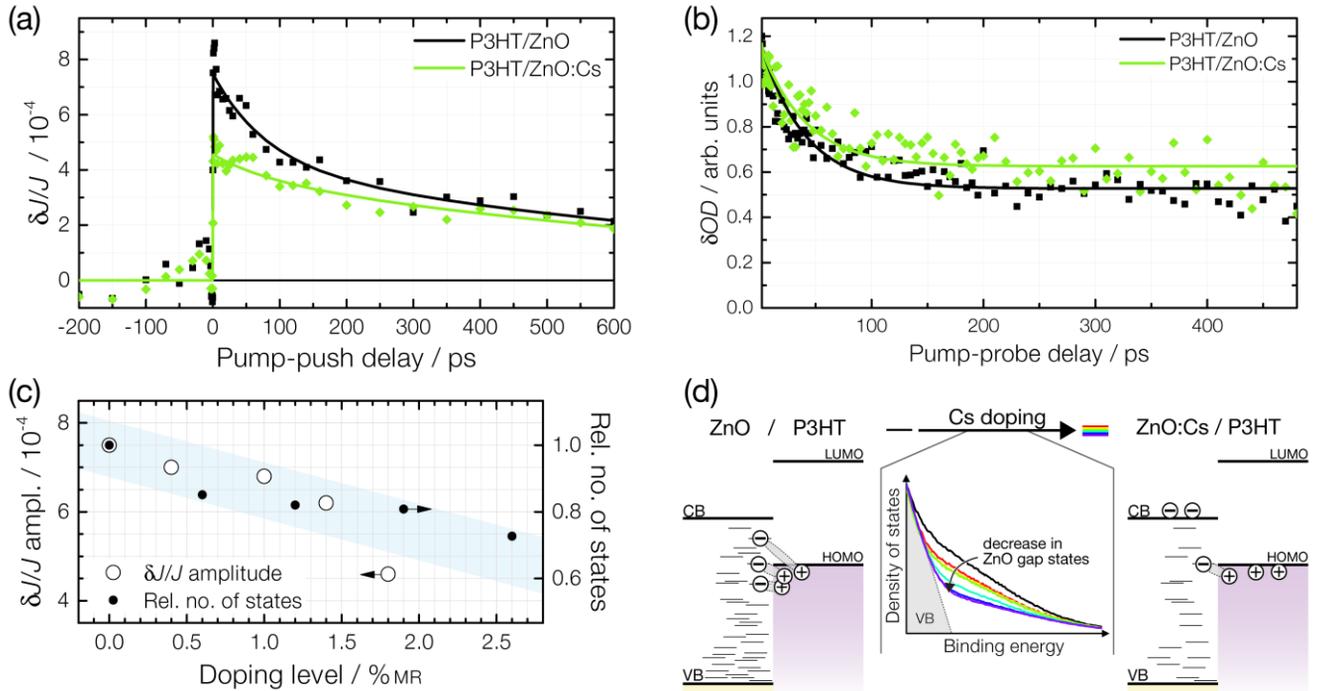
Figure 5: (a) Pump-push photocurrent measurements of an undoped photovoltaic device and the best device (1.8 % MR) to determine the amount of BCPs at the organic-inorganic interface. **(b)** Evaluation of the number of free charges in an undoped and doped ZnO (1.8 % MR). **(c)** Correlation between the yield of BCP states as determined by pump-push photocurrent measurements and the relative number of gap states from photoemission spectroscopy (Figure 3a). **(d)** Simplified model of the processes at the metal oxide/polymer interface after illumination by above-band-gap light, illustrating how a reduction of ZnO gap states by Cs doping leads to a smaller number of bound electron-hole pairs and more free charges.

To investigate the yield of bound charge pairs (BCPs) at the organic-inorganic interface, pump-push photocurrent measurements[25] were carried out on ZnO:Cs/P3HT photovoltaic devices for low Cs doping levels. In Figure 5a the change in photocurrent ($\delta J/J$) upon interaction with an IR push pulse is plotted over the delay between both pulses; this signal is proportional to the number of BCPs as a function of time after excitation. For the Cs doped sample, the number of BCPs is thus lower than in the undoped sample. Furthermore, a decrease in amplitude of ($\delta J/J$) was observed when increasing the

10

doping level (Figure 5c, open circles). This reduction is accompanied by the suppression of the fast decay component, which is presumably associated with the most tightly coupled BCP states promoted by the low-energy trapping sites at the oxide interface.[8] Therefore, the dissappearane of the fast component from the decay may indicate the suppression of the recombination dynamics, due to Cs passivation of interfacial trap states. As a result, in Cs doped ZnO, the formation of free charges is more efficient, due to fewer BCPs, leading to the higher photocurrent observed at low doping levels.

This picture is supported by the excited state dynamics at the ZnO:Cs/P3HT interface as observed by transient absorption spectroscopy (TA) experiments. The investigated samples were excited by a 600 nm pump pulse and photoinduced changes observed using a broadband supercontinuum probe pulse. The TA spectra (see Figure S6, SI) contained easily distinguishable ground-state bleach and stimulated emission contributions below 650 nm, as well as a photoinduced absorption band in the near IR (>700 nm) which is a well known optical fingerprint of charged states in organic semiconductors. Here, only the dynamics in this region are considered, not the early <2 ps kinetics as they can be affected by exciton-exciton anihilation in the P3HT films.[26] Figure 5b presents the TA kinetics of the charge-associated peak at 720 nm. The decays consist of two easily identifiable components: a fast component, reflecting the recombination of charged species; and, a slow component, corresponding to the long lived-charges. In agreement with pump-push photocurrent measurements, Cs doping leads to a relative increase of the long-lived component due to the improvement in generation of free charges. It is noted that the time scales observed in pump-push photocurrent and TA experiments are of similar order but do not match exactly. This disparity could be associated with the influence of external fields in the device, the effect of the high pump fluence in TA measurements, or slightly different sample morphology.

In a previously proposed model, electrons localized in defect states at the surface of the inorganic material coulombically attract hole polarons and thereby promote the formation of BCPs at the organic-inorganic interface.[4] The number of surface states can be extracted from the UPS spectra of the

11

ZnO:Cs layers (Figure 3a). Fewer states were observed (Figure 5c) for higher Cs doping levels: compared to the undoped ZnO the number of surface states is 19 % smaller in 1.9 %MR and 34 % smaller in 8.1 %MR Cs doped ZnO. This reduction in gap states correlates with the reduced ($\delta J/J$) amplitude upon Cs doping, as can be seen in Figure 5c. Thus, combining the results from pump-push photocurrent measurements (doping leading to a reduction in BCPs), from TA (doping leading to an increase in free charges), and UPS (doping leading to a reduction of surface gap states), not only explains the observation of increased J_{SC} at low doping levels, but also provides experimental proof for the proposed model of BCP creation, as illustrated in Figure 5d.

The *J-V* characteristics of an undoped ZnO and the best performing doped device (doping level 1.8 %MR) are presented in Figure 6 and their photovoltaic parameters are summarized in Table 1. The combination of the beneficial effect of doping on the bulk properties such as conductivity (which results in an increase in V_{OC}) and surface properties (which results in improved charge separation and improved J_{SC}) causes an overall 5-fold increase in the PCE of the hybrid bilayer device. For comparison, the P3HT/PCBM bilayer devices reported by Tada and coworkers – prepared using a contact transfer method which minimizes the interdiffusion of PCBM into P3HT[27–29] – had an overall PCE of 0.4 %. As shown in Figure 6 and Table 1, a 50 % higher performance was possible by using ZnO:Cs/P3HT. This comparison demonstrates that hybrid metal oxide/polymer systems can outperform the all organic polymer/fullerene system, once the process of charge separation is well understood.
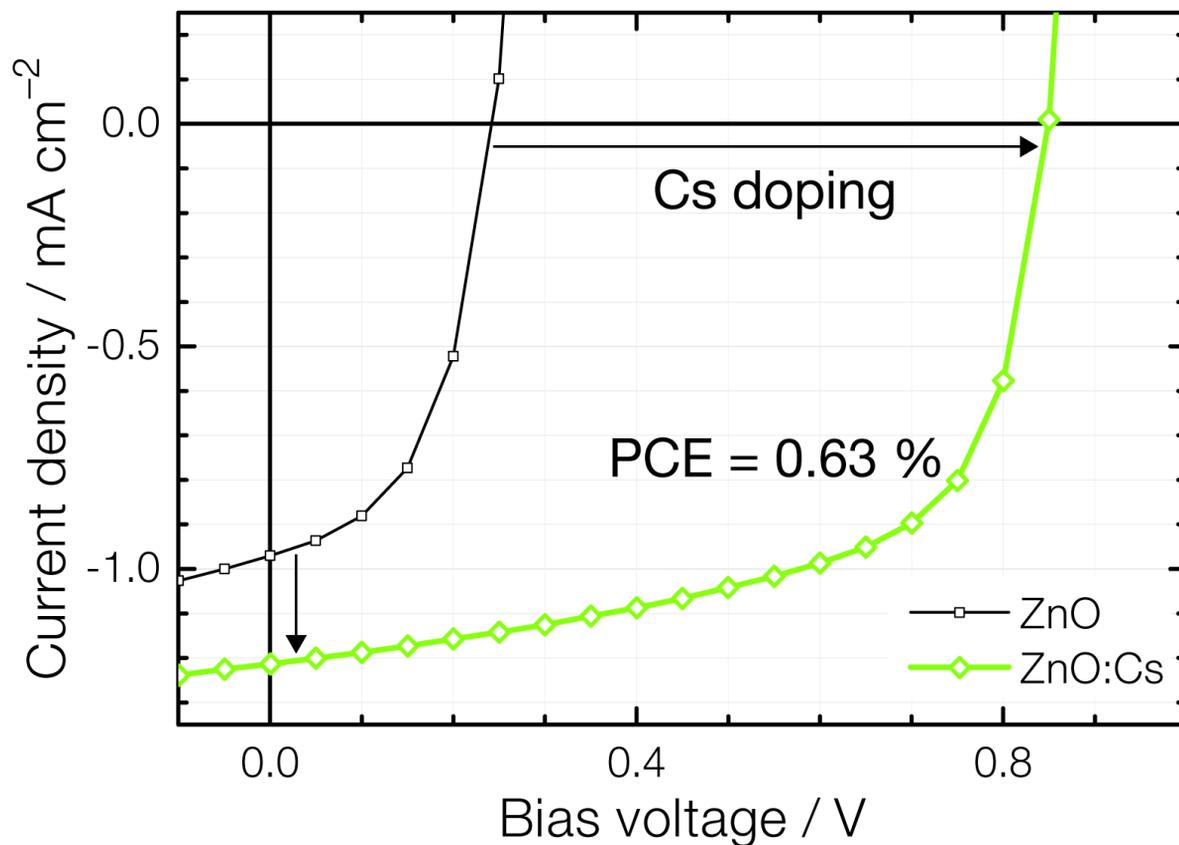
Figure 6: *J-V* characteristics of the best device (1.8 %MR Cs doped) compared to a representative undoped device from the same batch, measured under mismatch-corrected AM1.5G illumination.

Table 1: Comparison of PV parameters of undoped and Cs doped ZnO/P3HT photovoltaic devices and a P3HT/PCBM bilayer device by Tada et al. where interdiffusion was minimized by a direct transfer method.

	V_{OC} / V	J_{SC} / mA cm^{-2}	FF / %	PCE / %
P3HT/ZnO	0.24	0.97	49	0.12
P3HT/PCBM (Tada et al.)[15]	0.50	1.51	53	0.40
P3HT/ZnO:Cs	0.85	1.21	61	0.63

Conclusion

It was demonstrated in this study that the introduction of Cs as a dopant into the ZnO layer of hybrid bilayer photovoltaic devices can lead to a considerable increase in device performance. As shown in Figure 6, Cs doped devices can achieve power conversion efficiencies higher than in bilayer P3HT/PCBM cells fabricated using a direct transfer method, where the intermixing of donor and acceptor is minimized.[15]

The improved performance was not only due to the increased open circuit voltage upon Cs doping but – unlike with Ca, Mg or Sr as a dopant – is also caused by an increased short circuit current due to a smaller number of bound charge pairs at the interface. While with Sr doping a self assembled monolayer at the charge separating surface was the origin of higher short circuit current,[8] and in the case of Mg[5] and Ca[9] an increased surface area was the cause of higher charge separation, the Cs doped ZnO exhibited better charge extraction and higher device currents without the need for a surface modifier or morphological changes to the interface. Combining the positive effect of Cs doping of the inorganic layer on the open circuit voltage with techniques to further improve device current – such as nano structuring or bulk heterojunction morphologies – may contribute to hybrid photovoltaic devices with higher power conversion efficiencies.

Furthermore, by means of Cs doping of a hybrid model system, it was found that the yield of bound charge pairs at the organic-inorganic interface is proportional to the density of gap states at the metal oxide surface, which for the first time gives direct experimental evidence for the previously proposed model of bound charge pair creation.[4]

Materials and Methods

Sol-gel deposition of Cs doped ZnO layers

Sol-gel preparation.

Adapted from Kwon et al.[30], the undoped ZnO sol-gel was prepared by dissolving $0.46 \, \text{mol} \, l^{-1}$ zinc acetate dihydrate (99.999 %, Aldrich) and $0.46 \, \text{mol}^{-1}$ monoethanolamine ($\geq$ 99.5 %, Aldrich) in 2-methoxyethanol (anhydrous, 99.8 %, Aldrich). Doping was accomplished by adding Cs_2CO_3 (99.995 %, Aldrich) to the solution in molar ratios (#Cs atoms / #Zn atoms) of up to 10 %MR. The solution was heated to 70°C and stirred until fully dissolved.

Sol-gel deposition.

For the preparation of photovoltaic devices, patterned ITO/glass substrates were used; the examination of only the metal oxide layer was done on films deposited on glass, ITO/glass or Si substrates. The substrates were cleaned by successive sonication in acetone and isopropanole, followed by an O_2 plasma treatment.

Using the prepared sol-gel, a single layer was spin-coated onto the substrate (45 s at 2000 rpm) and annealed for 25 min at 200°C under air. This resulted in films of $(50 \pm 5) \, \text{nm}$ thickness (as determined by Dektak profilometer). After a cool down period of 10 min to 70°C, the samples were transferred into a nitrogen atmosphere ($O_2 < 2$ ppm, $H_2O < 1$ ppm), where the remaining steps of fabrication followed.

Fabrication of photovoltaic devices

A solution of 10 $\text{mg} \, \text{ml}^{-1}$ regioregular Poly-[3-hexylthiophene] (1-Material) in chlorobenzene (anhydrous, Sigma Aldrich) was filtered ($d < 0.45 \, \mu\text{m}$) and spin-coated (45 s at 2000 rpm) onto the metal oxide layer. Eight anode contacts per substrate were formed by thermal evaporation of 7 nm of MoO_3

and 80 nm of Ag under high vacuum ($p < 10^{-6}$ mbar). Deposition rates were 0.05 nm s^{-1} and 0.1 nm s^{-1} respectively and the area of a single anode contact was 4.5 mm^2.

The devices were then post-annealed at 140°C for 10 min and left to cool down to room temperature. To reduce environmental effects, a cover glass was fixed to the anode side using a slow-setting two-component epoxy adhesive.

Device and film characterization

Characterization of photovoltaic devices.

Current-voltage characteristics of photovoltaic devices were measured using a Keithley 2450 Source Measure Unit. Light IV curves were recorded under 100 mW cm^{-2} AM 1.5G lighting conditions using a ABET Sun 3000 class AAA solar simulator, which was adjusted in intensity to compensate for the spectral mismatch between the spectral output, and the spectral response of both the ZnO:Cs/P3HT device and the reference Si cell (NIST traceable, VLSI). The spectral mismatch for all measurements was ≤3 %. EQE measurements (Fig S3, SI) were made with monochromatic light (approximately 5 nm bandwidth), and referenced to a NIST traceable Si photodiode (Thorlabs). To examine exciton dissociation of photovoltaic devices and bound charge pairs, a pump-push photocurrent technique was employed.[25]

Characterization of ZnO:Cs and P3HT/ZnO:Cs films.

Optical transmission spectra were acquired with a Jasco UV-670 spectrophotometer in the range from 800 nm to 270 nm and the spectrum of the substrate was substracted. The optical band gap was determined by calculating the intercept of linear fits to the background and the absorption onset.

Films for investigation of surface morphology were prepared on ITO/glass substrates. A Veeco NanoScope II atomic force microscope in tapping mode was used to record height maps of the samples in multiple areas of the sample.

To determine the conductivity of undoped and doped ZnO films, four pairs of Al electrodes ($500\,\mu m$ apart, $2500\,\mu m$ wide) were thermally evaporated onto the deposited layer using a shadow mask and an encapsulation glass was added. After exposure to solar simulator light, the current at $1\,V$ bias voltage was measured using the Keithley 2450 Source Measure Unit. Knowing the thickness of the films (from a Dektak profilometer) and the geometry of the electrodes, the conductivity was calculated. The error bars show the standard error of the mean of representative pairs of electrodes on the same substrate.

Chemical composition was examined using X-ray photoelectron spectroscopy (XPS). Ultraviolet photoelectron spectroscopy (UPS) was used to determine the ionization potential and surface DOS of ZnO:Cs films. Samples for XPS and UPS were fabricated on Si substrates and transferred into the photoemission system's ultrahigh vacuum chamber (ESCALAB 250Xi). XPS measurements were performed using an XR6 monochromated Al Kα source ($1486.6\,eV$) and a pass energy of $20\,eV$. A double-differentially pumped He gas discharge lamp (He I, $hv = 21.22\,eV$) with a pass energy of $2\,eV$ was used in UPS measurements.

Population dynamics at the P3HT/ZnO:Cs interface were studied using transient absorption spectroscopy (TA). The layers were prepared in the same procedure as the devices, but with a thinner P3HT layer (~$10\,nm$) and on UV grade fused silica (Spectrosil) substrates, and were UV-exposed for $3\,min$. The output of a regeneratively amplified Ti:Sa laser generating $100\,fs$ pulses with a repetition rate of $1\,kHz$ was divided into two parts: for the probe beam, $1\,\%$ of the intensity was used to generate white light (in a $2\,mm$ Sapphire crystal, 450-750 nm); to generate the pump beam, the remaining $99\,\%$-intensity beam was sent into a non-collinear optical parametric amplifier. The latter was centered at $600\,nm$ and showed a pulse duration of $16\,fs$ after compressing it by means of a prism compressor. Every second pump beam was blocked with a synchronized chopper wheel in order to get difference

spectra, i.e. with and without excitation. The excitation beam was attenuated to pulse energies of $30\,nJ$ with a focal spot diameter of approximately $200\,\mu m$ ($\sim 3 \cdot 10^{12}$ photons cm^{-2}) resulting in photon flux of $1\,\mu J\ cm^{-2}$. Pump and probe beams were focused onto the substrate under normal air conditions. To account for differences in the preparation process of the samples, the TA spectra were normalized to the peak of the ground state bleach.

Acknowledgements

Associated Content

The supplemental information (SI) includes the following figures and tables:

XPS spectra of Cs doped ZnO films and determination of Cs doping level (Figure S1);

Photovoltaic metrics for a range of different doping levels (Figure S2);

Table of photovoltaic metrics corresponding to Figure S2 (Table ST1);

EQE measurements of devices with different doping levels (Figure S3);

Determination of ionization potential and optical band gap from UPS and UV-vis (Figure S4);

AFM micrographs, surface roughness and surface area over doping level (Figure S5);

Transient Absorption spectroscopy measurements at different times of pump-probe delay (Figure S6).

References

[1]   M. Wright, A. Uddin, *Sol. Energy Mater. Sol. Cells* **2012**, *107*, 87.

[2]   Y. Vaynzof, D. Kabra, T. J. K. Brenner, H. Sirringhaus, R. H. Friend, *Isr. J. Chem.* **2012**, *52*, 496.

[3]   H. Li, P. Winget, J. L. Brédas, *Chem. Mater.* **2014**, *26*, 631.

[4]   Y. Vaynzof, A. a. Bakulin, S. Gélinas, R. H. Friend, *Phys. Rev. Lett.* **2012**, *108*, 246605.

[5]   D. C. Olson, S. E. Shaheen, M. S. White, W. J. Mitchell, M. F. a. M. van Hest, R. T. Collins, D. S. Ginley, *Adv. Funct. Mater.* **2007**, *17*, 264.

[6]   R. L. Z. Hoye, K. P. Musselman, J. L. Macmanus-Driscoll, *APL Mater.* **2013**, *1*, DOI 10.1063/1.4833475.

[7]   K. P. Musselman, S. Albert-Seifried, R. L. Z. Hoye, A. Sadhanala, D. Muñoz-Rojas, J. L. MacManus-Driscoll, R. H. Friend, *Adv. Funct. Mater.* **2014**, *24*, 3562.

[8]   O. Pachoumi, A. Bakulin, A. Sadhanala, H. Sirringhaus, R. H. Friend, Y. Vaynzof, *J. Phys. Chem. C* **2014**, *118*, 18945.

[9]   M. Wang, J. P. Sun, S. Suei, I. G. Hill, *J. Appl. Phys.* **2012**, *112*, 0.

[10]   Y. Vaynzof, D. Kabra, L. Zhao, P. K. H. Ho, A. T. S. Wee, R. H. Friend, *Appl. Phys. Lett.* **2010**, *97*, 033309.

[11]   C. Goh, S. R. Scully, M. D. McGehee, *J. Appl. Phys.* **2007**, *101*, DOI 10.1063/1.2737977.

[12]   Y. Y. Lin, Y. Y. Lee, L. Chang, J. J. Wu, C. W. Chen, *Appl. Phys. Lett.* **2009**, *94*, DOI 10.1063/1.3080203.

[13]   J. Weickert, F. Auras, T. Bein, L. Schmidt-Mende, *J. Phys. Chem. C* **2011**, *115*, 15081.

[14]   J. Weickert, E. Zimmermann, J. B. Reindl, T. Pfadler, J. a Dorman, A. Petrozza, L. Schmidt-mende, *APL Mater.* **2013**, *1*, 042109.

[15]   A. Tada, Y. Geng, Q. Wei, K. Hashimoto, K. Tajima, *Nat. Mater.* **2011**, *10*, 450.

[16]   R. L. Z. Hoye, B. Ehrler, M. L. Böhm, D. Muñoz-Rojas, R. M. Altamimi, A. Y. Alyamani, Y. Vaynzof, A. Sadhanala, G. Ercolano, N. C. Greenham, R. H. Friend, J. L. MacManus-Driscoll, K. P. Musselman, *Adv. Energy Mater.* **2014**, *4*, 1.

[17]   A. Kahn, N. Koch, W. Gao, *J. Polym. Sci. Part B Polym. Phys.* **2003**, *41*, 2529.

[18]   Y. Vaynzof, D. Kabra, L. L. Chua, R. H. Friend, *Appl. Phys. Lett.* **2011**, *98*, 30.

[19]   M. C. Gwinner, Y. Vaynzof, K. K. Banger, P. K. H. Ho, R. H. Friend, H. Sirringhaus, *Adv. Funct. Mater.* **2010**, *20*, 3457.

[20]   J.-L. Bredas, *Mater. Horiz.* **2014**, *1*, 17.

[21]   D. C. Look, *Mater. Sci. Eng. B Solid-State Mater. Adv. Technol.* **2001**, *80*, 383.

[22]   M. Dvorak, S. H. Wei, Z. Wu, *Phys. Rev. Lett.* **2013**, *110*, 1.

[23]   Y. Liu, Y. Li, H. Zeng, *J. Nanomater.* **2013**, *2013*, DOI 10.1155/2013/196521.

[24]   R. L. Z. Hoye, D. Muñoz-Rojas, K. P. Musselman, Y. Vaynzof, J. L. MacManus-Driscoll, *ACS Appl. Mater. Interfaces* **2015**, 150515102727002.

[25]   A. Bakulin, A. Rao, Y. Vaynzof, S. Gelinas, V. G. Pavelyev, P. H. M. van Loosdrecht, M. S. Pshenichnikov, D.

Niedzialek, J. Cornil, D. Beljonne, R. H. Friend, *EPJ Web Conf.* **2013**, *41*, 05020.

[26]   J. Piris, T. E. Dykstra, A. a. Bakulin, P. H. M. Van Loosdrecht, W. Knulst, M. T. Trinh, J. M. Schins, L. D. a Siebbeles, *J. Phys. Chem. C* **2009**, *113*, 14500.

[27]   B. A. Collins, E. Gann, L. Guignard, X. He, C. R. Mcneill, H. Ade, *Phys. Chem. Lett.* **2010**, 3160.

[28]   B. A. Collins, J. R. Tumbleston, H. Ade, *Phys. Chem. Lett.* **2011**.

[29]   N. D. Treat, M. a. Brady, G. Smith, M. F. Toney, E. J. Kramer, C. J. Hawker, M. L. Chabinyc, *Adv. Energy Mater.* **2011**, *1*, 82.

[30]   S. Kwon, K.-G. Lim, M. Shim, H. C. Moon, J. Park, G. Jeon, J. Shin, K. Cho, T.-W. Lee, J. K. Kim, *J. Mater. Chem. A* **2013**, *1*, 11802.

Supplemental Information
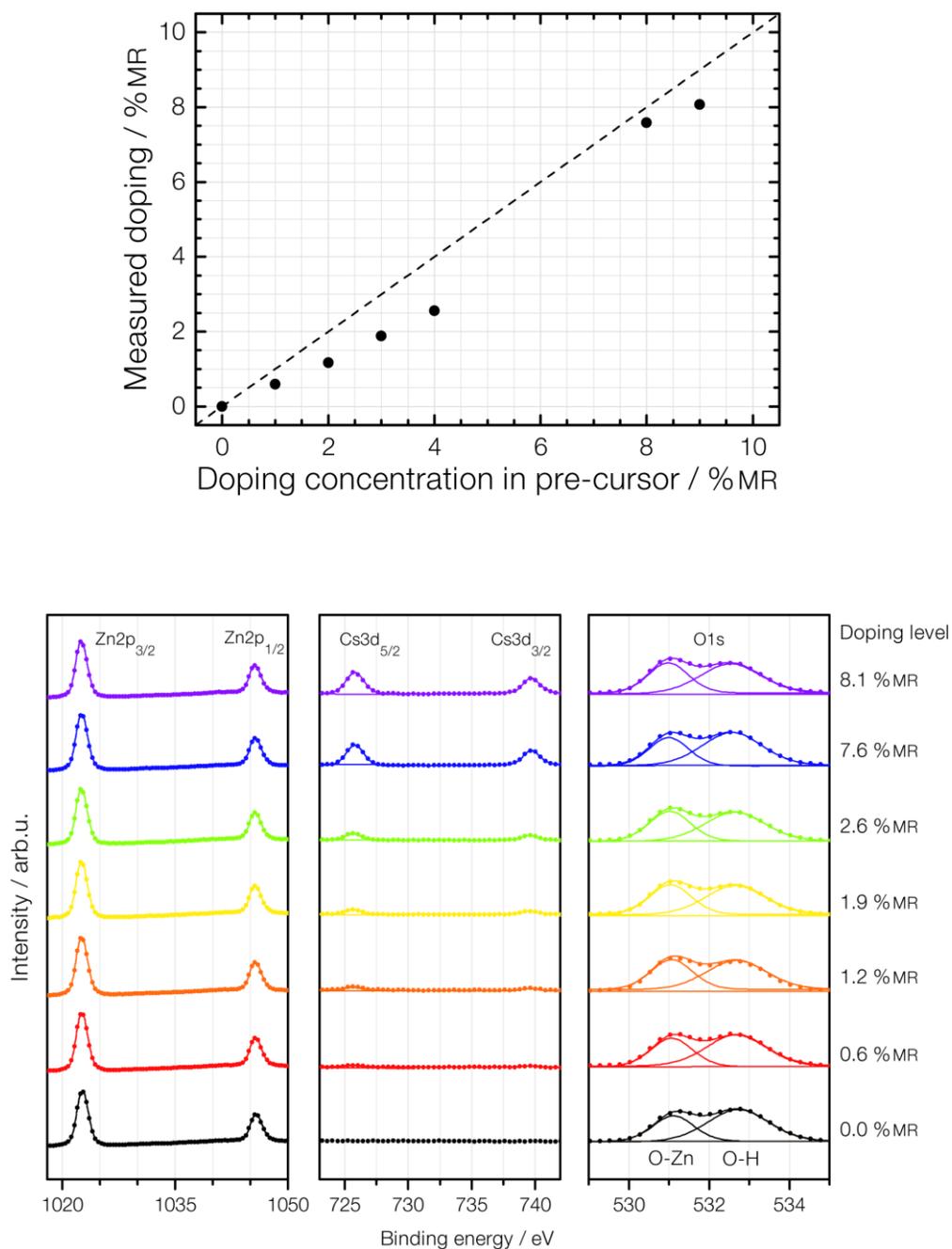
Figure S1:   Determination of Cs doping level by X-ray photoemission spectroscopy (XPS) of Cs doped ZnO films. The first figure shows the doping level determined by XPS over the doping level expected from sol-gel preparation; the bottom figure gives the corresponding XPS spectra.
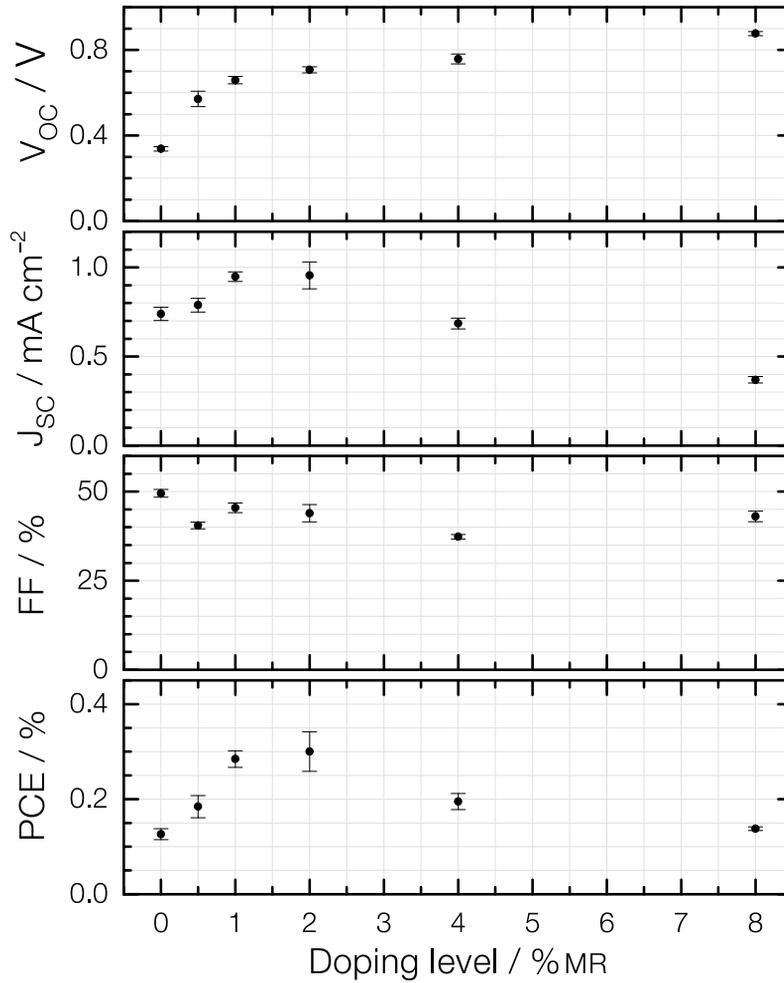
Figure S2: Mean values and standard errors for photovoltaic metrics measured from 26 devices from the same batch (4-5 per doping level) under mismatch-corrected AM 1.5G conditions with $100\,mW\,cm^{-2}$ light intensity. The monotonic increase in open circuit voltage as well as the initial increase and final decrease in short circuit current can be seen; combined, that leads to a peak power conversion efficiency at 2 %MR.

Table ST1: Mean values and standard errors for photovoltaic performance summarized in Figure S2.

Doping level / %MR	V_{OC} / V	J_{SC} / mA cm^{-2}	FF / %	PCE / %
0	0.34 ± 0.01	0.74 ± 0.04	49 ± 1	0.13 ± 0.01
0.5	0.57 ± 0.04	0.79 ± 0.04	41 ± 1	0.18 ± 0.02
1	0.66 ± 0.02	0.95 ± 0.03	45 ± 1	0.28 ± 0.02
2	0.71 ± 0.01	0.96 ± 0.08	44 ± 2	0.30 ± 0.04
4	0.76 ± 0.02	0.69 ± 0.03	37 ± 1	0.20 ± 0.02
8	0.88 ± 0.01	0.37 ± 0.02	43 ± 1	0.14 ± 0.01
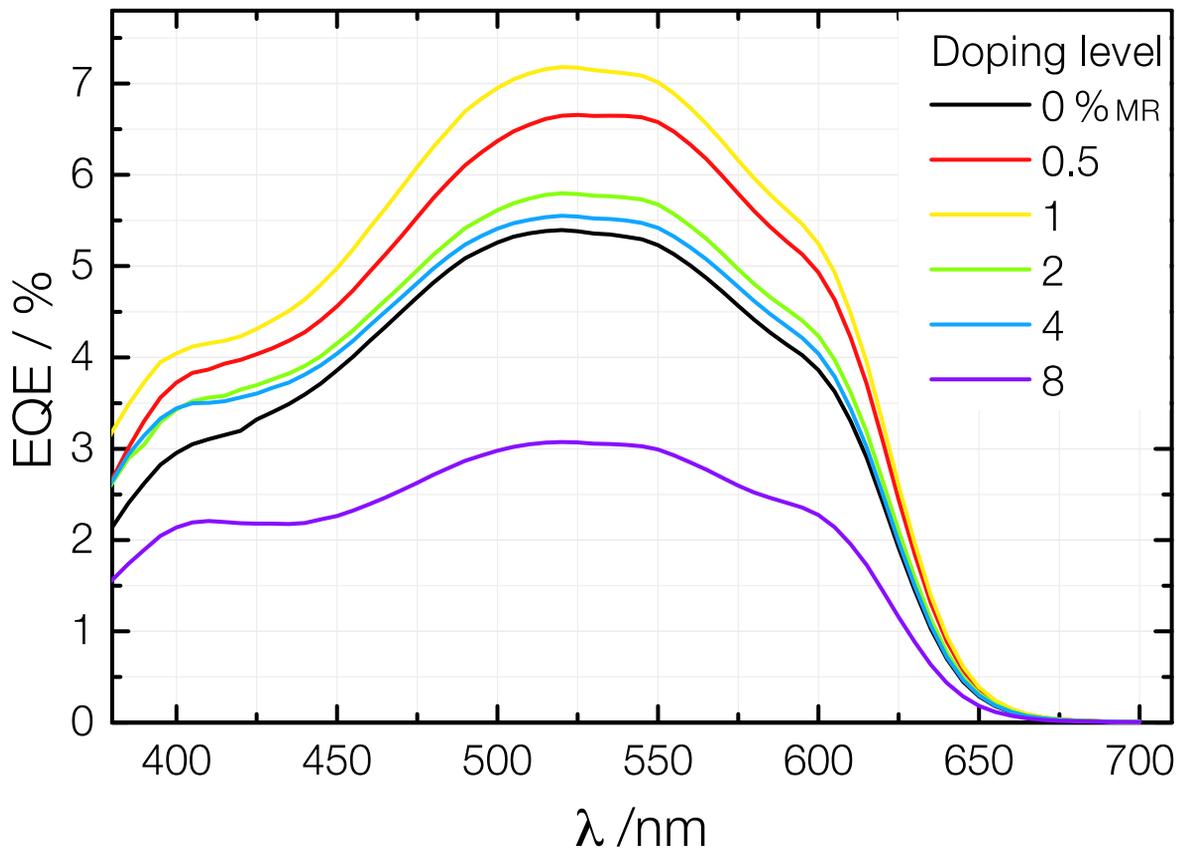
Figure S3: External Quantum Efficiency (EQE) measurements of devices with different doping levels show no change in the spectrum upon doping, but – as expected – exhibit the same trend in the magnitude of the signal as in the J_{SC} photovoltaic metric: for low doping levels, the photocurrent is higher than in the undoped case, while at high doping levels it decreases again. Note that the spectra shown here are not from the same set of devices as those shown in Figure 2; in this case, the highest J_{SC} was found for a doping level of 1 %MR.
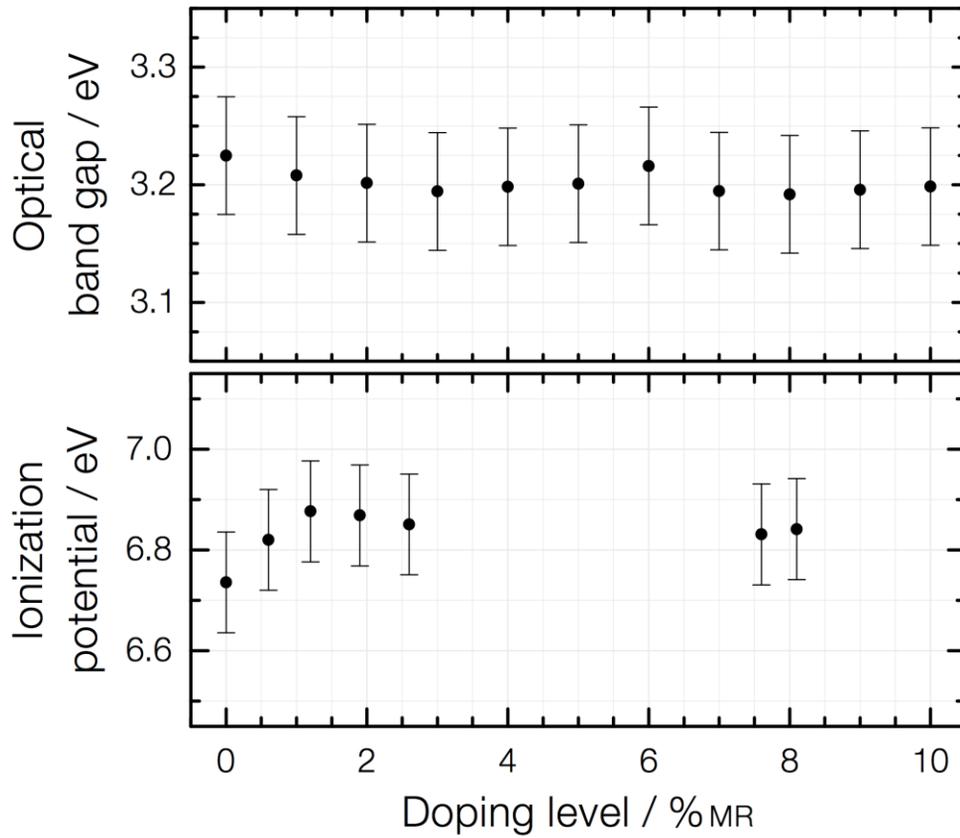
Figure S4: Optical band gap (E_g) and Ionization potential (IP) as extracted from UPS and UV-vis spectra respectively, see Figure 3. Within the uncertainty of the measurements and fitting procedure, neither E_g nor IP change substantially with the introduction of Cs as a dopant. Hence, the change in open circuit voltage of corresponding photovoltaic devices can not have been due to a change in energetic structure of the device.
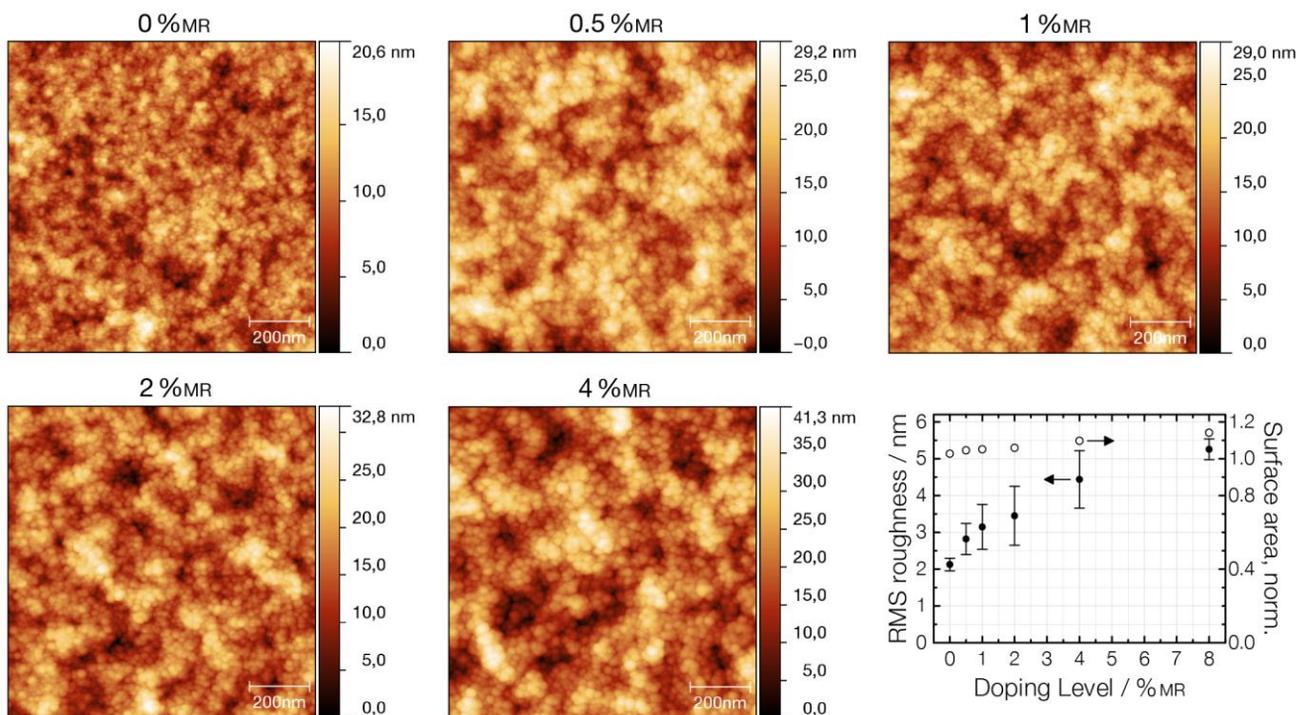
Figure S5: ZnO:Cs film surface morphology measured using atomic force microscopy (AFM) in tapping mode. Shown are $1\,\mu m^2$ height maps of representative areas of the sample. The graph presents average characteristic data of several measurements. The error bars show the standard deviation; for the surface area, the standard deviation is smaller than the size of the circles.
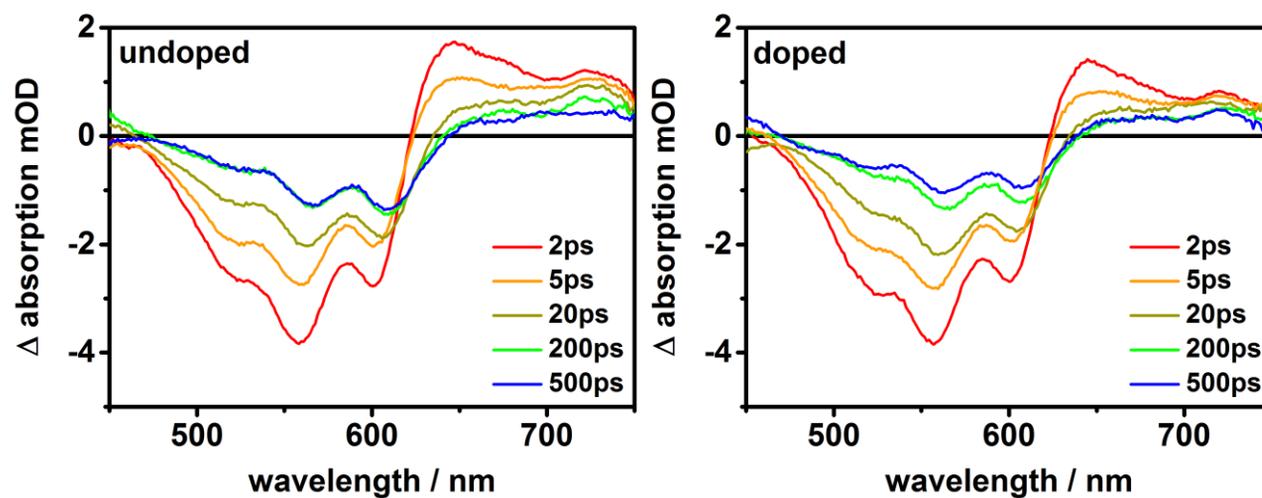
Figure S6: Transient absorption spectra of P3HT/ZnO and P3HT/ZnO:Cs samples (2%MR), measured at different pump-probe delays.